

A graph of dark energy significance on different spatial and mass scales (Research Note)

P. Teerikorpi¹, P. Heinämäki¹, P. Nurmi¹, A.D. Chernin², M. Einasto³, M. Valtonen¹, and G. Byrd⁴

¹ Tuorla Observatory, Department of Physics and Astronomy, University of Turku, 21500 Piikkiö, Finland

² Sternberg Astronomical Institute, Moscow University, Moscow, 119899, Russia

³ Tartu Observatory, 61602, Tõravere, Estonia

⁴ University of Alabama, Tuscaloosa, AL 35487-0324, USA

Received / Accepted

ABSTRACT

Context. The current cosmological paradigm sees the formation and evolution of the cosmic large-scale structure as governed by the gravitational attraction of the Dark Matter (DM) and the repulsion of the Dark Energy (DE).

Aims. We characterize the relative importance of uniform and constant dark energy, as given by the Λ term in the standard Λ CDM cosmology, in galaxy systems of different scales, from groups to superclusters.

Methods. An instructive " Λ significance graph" is introduced where the matter-DE density ratio $\langle \rho_M \rangle / \rho_\Lambda$ for different galaxy systems is plotted against the radius R . This presents gravitation and DE dominated regions and shows directly the zero velocity radius, the zero-gravity radius, and the Einstein-Straus radius for any fixed value of mass.

Results. Example galaxy groups and clusters from the local universe illustrate the use of the Λ significance graph. These are generally located deep in the gravity-dominated region $\langle \rho_M \rangle / \rho_\Lambda > 2$, being virialized. Extended clusters and main bodies of superclusters can reach down near the border line between gravity-dominated and DE dominated regions $\langle \rho_M \rangle / \rho_\Lambda = 2$. The scale-mass relation from the standard 2-point correlation function intersects this balance line near the correlation length.

Conclusions. The $\log \langle \rho_M \rangle / \rho_\Lambda$ vs. $\log R$ diagram is a useful and versatile way to characterize the dynamical state of systems of galaxies within the Λ dominated expanding universe.

Key words. cosmology: dark matter, dark energy

1. Introduction

According to the standard Λ CDM cosmology, a great majority of the material contents of the universe or about 95 per cent in energy density, is made of unknown dark substances called dark matter and dark energy (DE).

Dark matter is revealed by its gravitation, while dark energy (represented by Einstein's cosmological constant Λ in standard cosmology) is an "antigravitating" uniform vacuum-like fluid. The DE background produces antigravity. It is stronger than matter gravity in the present universe as a whole, making the universal expansion accelerate.

According to the Planck Surveyor results (Planck Collaboration 2013), the global density of the DE is, in round numbers, $\rho_\Lambda \approx 6 \times 10^{-30} \text{ g cm}^{-3}$.¹

Because of the non-uniform distribution of gravitating matter, the cosmic antigravity can be stronger than gravity also locally on scales of $\sim 1 - 10 \text{ Mpc}$ (Chernin 2001), which in principle makes it possible to detect the DE in the local galaxy universe, as reviewed by Byrd et al. (2012, 2015). For a recent study about the DE in the vicinity of the Local Group, see Saarinen & Teerikorpi (2014).

¹ The difference from the previous WMAP value ($\approx 7 \times 10^{-30} \text{ g cm}^{-3}$) is mainly caused by the smaller value of the Hubble constant ($h = 0.67$), lowering the critical density ($1.88h^2 \times 10^{-30} \text{ g cm}^{-3}$) which is now equal to $\rho_{\text{crit}} = 8.52 \times 10^{-30} \text{ g cm}^{-3}$.

The presence of DE along with gravitating matter influences the formation of the large scale structure on all scales from groups of galaxies to superclusters. In regions where the DE dominates over the gravitating matter, new structures do not condense and linear perturbations of density decay (or even non-linear if sheet-like Chernin et al. 2003). The antigravity of DE also puts an upper limit on the size of a bound system of a certain mass and it influences dynamic mass determinations, leading to too low a mass Chernin et al. (2009, 2012).

It occurs that a useful parameter which characterizes the influence of DE is the energy density ratio $\langle \rho_M \rangle / \rho_\Lambda$ as calculated for the system or scale under inspection.

In the present Note, we introduce a graph presenting the ratio $\langle \rho_M \rangle / \rho_\Lambda$ for systems of different size and mass. This diagram displays in a direct way a few relevant scales which appear for each fixed mass of a spherical or slightly flattened system in Λ CDM cosmology. The location of a galaxy system in the diagram indicates whether its overall dynamics is dominated by gravity or DE antigravity. This Λ significance graph has also limited use for flattened systems.

2. Zero-gravity radius and Einstein-Straus scale

A natural scale which appears around a mass point (or a spherically symmetric system) embedded in the dark en-

ergy background, is the zero-gravity radius R_{ZG} . In a weak field situation one may write (Chernin et al. 2009) the force affecting a test particle with mass m as the sum of Newton's gravity force produced by the mass M and Einstein's anti-gravity force due to DE:

$$F(R) = \left(-\frac{GM}{R^2} + \frac{8\pi G}{3}\rho_\Lambda R \right) m. \quad (1)$$

At the zero-gravity distance $R = R_{ZG}$ (Chernin 2001):

$$R_{ZG} = \left(\frac{M}{\frac{8\pi}{3}\rho_\Lambda} \right)^{1/3} = 1.1 \text{ Mpc} \times \left(\frac{M/10^{12}M_\odot}{\rho_\Lambda/6 \times 10^{-30} \text{ g/cm}^3} \right)^{1/3} \quad (2)$$

gravity is equal to antigravity.

Another interesting scale is related to the Einstein-Straus radius R_{ES} . This comes from the central mass plus vacuole solution by Einstein & Straus (1945), where the radius of the vacuole is such that the mean density within it is equal to the current density of the Friedmann universe:

$$R_{ES} = [M/(\frac{4\pi}{3}\rho_m)]^{1/3} = R_{ZG}(2\frac{\rho_\Lambda}{\rho_m})^{1/3} \simeq 1.7R_{ZG} \quad (3)$$

This may be imagined as the radius of the spherical volume from which the mass making up the system has been gathered in the past during the gravitational instability process.

Dark energy puts an absolute upper limit on the size of a gravitationally bound system: it must be located within its zero-gravity sphere where gravity dominates.

3. Matter-to-DE ratio vs. scale diagram

It is instructive and useful to construct a diagram where the x -axis is the logarithm of the spatial scale (or the radius of a system) and the y -axis gives the (log) ratio of the average density $\langle \rho_M \rangle$ of a system and the (constant) DE density equal to the global value ρ_Λ .

For $\rho_\Lambda \approx 6 \times 10^{-30} \text{ g cm}^{-3}$, the ratio $\langle \rho_M \rangle / \rho_\Lambda$ becomes

$$\langle \rho_M \rangle / \rho_\Lambda = 2.7 \frac{(M/10^{12}M_\odot)}{(R/\text{Mpc})^3} \quad (4)$$

where M is the mass within the radius R . In logarithms:

$$\log \langle \rho_M \rangle / \rho_\Lambda = 0.43 + \log M/10^{12}M_\odot - 3 \times \log R/\text{Mpc} \quad (5)$$

In the $\log \langle \rho_M \rangle / \rho_\Lambda$ vs. $\log R$ diagram this relation forms a family of inclined straight lines for each fixed value of the mass M . Fig. 1 explains the meaning of the different lines and regions in such a diagram. Note that the fraction of the DE density grows when one goes downwards in the diagram.

In the upper part of the diagram, the systems are dominated by gravitation. They may be bound and for sufficiently high $\langle \rho_M \rangle / \rho_\Lambda$ they can be virialized (Sect.5).

We show in Fig.1 the horizontal line giving the zero-velocity radius R_{ZV} when intersecting the inclined constant mass line. This density ratio is obtained from the classical relation between M and R_{ZV}

$$M = \frac{\pi^2}{8G} t_0^{-2} R_{ZV}^3 = 2.74 \times 10^{12} M_\odot \left(\frac{t_0}{10^{10} \text{ yrs}} \right)^{-2} \left(\frac{R_{ZV}}{1 \text{ Mpc}} \right)^3 \quad (6)$$

by Lynden-Bell (1981). In addition, the effect of Λ increases R_{ZV} by about 1.15, or the inferred mass by about 1.5 (Peirani & de Freitas Pacheco 2006; Saarinen & Teerikorpi 2014; Tully 2015). The calculation leads to $\log \frac{\langle \rho_M \rangle}{\rho_\Lambda} \approx 0.75$.

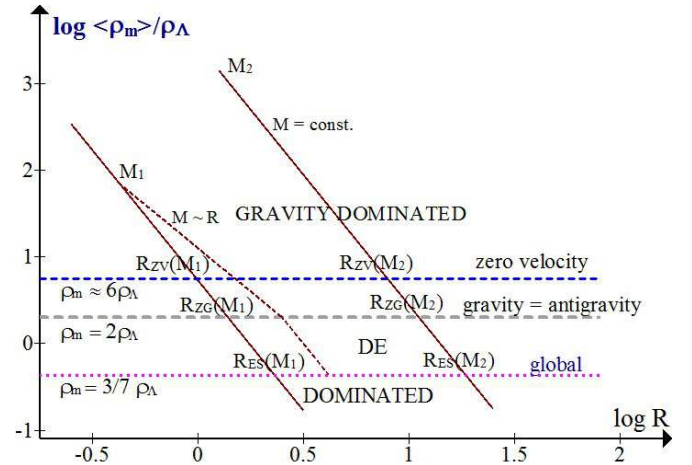


Fig. 1. $\log \langle \rho_M \rangle / \rho_\Lambda$ vs. $\log R$ for spherical systems. The inclined lines correspond to different mass values. Above the middle "gravity = antigravity" line the region is dynamically dominated by gravitation, below this line by DE. Intersections give the radii R_{ZV} , R_{ZG} , and R_{ES} . Dotted inclined lines illustrate the case when the mass increases with the radius (see the text).

The lower part of the diagram contains two horizontal lines. One is for the ratio $\langle \rho_M \rangle / \rho_\Lambda = 2$ (gravity = antigravity). The second one is for the global matter-to-DE ratio 0.43. Spherical systems below the upper line are dynamically dominated by the antigravitating DE background.

When we consider systems of a fixed mass M and go down along the inclined straight line (Eq.(5)), it intersects the upper line at the zero-gravity radius $R_{ZG}(M)$ (Eq.(2)), which also is the maximal possible size of a bound system.

For systems below the upper horizontal line the radius of the system exceeds the zero-gravity radius. Then the system is not gravitationally bound as a whole. Note, however, that this is valid for a spherical system.

Furthermore, the point of intersection with the "global" line gives formally the Einstein-Straus radius R_{ES} for this same central mass (Eq.(3)). This is also the distance where the Hubble flow around the mass reaches the global Hubble expansion rate (Teerikorpi & Chernin 2010). Below the global line, there is matter underdensity.

In a perfectly uniform Friedmann model, only the points of the global line exist. Then R refers to the current size of a comoving volume containing the matter mass M .²

In Fig.1 we have also shown what happens if the mass of a system is M_1 as measured within a radius R_1 , and then increases (e.g., $M \propto R$), up to a zero-gravity radius R'_{ZG} , the absolute upper limit for the size of a bound system. Chernin et al. (2012) considered such a situation for galaxy groups using different mass-radius laws (density profiles).

² If we calculate R_{ZG} around a point in a homogenous world from Eq.(2), this radius will increase directly proportional to the radius of the considered matter sphere. This means that one cannot ascribe physical significance to the zero-gravity radius within a fully uniform universe – every point is as it were on the surfaces of a great number of zero-gravity spheres of arbitrarily different sizes, not feeling any force.

4. Example systems of galaxies

To illustrate the meaning of the $\langle \rho_M \rangle / \rho_\Lambda$ vs. scale diagram, we calculate for several well-known galaxy systems (listed below) the ratio $\langle \rho_M \rangle / \rho_\Lambda$ and put them in the $\langle \rho_M \rangle / \rho_\Lambda$ vs. $\log R$ diagram of Fig.2.

In some cases we plot the results for two or more increasingly large radii around the system. The mass and size values are characteristic rather than accurate.

The Local Group. The mass of the LG has notable uncertainty, with values cited from 1.5 to about $4 \times 10^{12} M_\odot$ (e.g., van den Bergh 1999; Chernin et al. 2009; Partridge et al. 2013). Here we use the mass value $2 \times 10^{12} M_\odot$ and the radius $R = 1.0$ Mpc. Also, we have plotted the zero-gravity region, $R_{ZG} = 1.4$ Mpc, in order to illustrate its location at the intersection of the two lines as noted above.

The Local Sheet. This local flattened system comprises, in addition to the Local Group, other groups and galaxies within about 6 Mpc and seems to form a dynamically separate system, not being just an arbitrarily defined part of the plane of the Local Supercluster. McCall (2014) estimates its mass as about 2.7 times that of the LG, or in our diagram $5.4 \times 10^{12} M_\odot$, within the radius of 3.75 Mpc.

The Fornax Cluster. For an inner part of this cluster ("Fornax₁" in our diagram) we use the virial mass $7 \times 10^{13} M_\odot$ (Drinkwater et al. 2001) for $R_{vir} = 1.4$ Mpc. Using a Tolman-Bondi infall model (with Λ), Nasonova et al. (2011) derived $2.2 \times 10^{14} M_\odot$ within 4.6 Mpc ("Fornax₂").

Virgo and the Local Supercluster. For the central part of the LSC, the Virgo cluster ("Virgo₁"), we use its virial mass $\sim 1 \times 10^{15} M_\odot$ within 2 Mpc (e.g., Teerikorpi et al. 1992; Ekhholm et al. 2000). Within the LG distance (18 Mpc) ("Virgo₂"), the mass is about $5 \times 10^{15} M_\odot$, from a TB analysis (Ekhholm et al. 2000).

The Coma Cluster. Chernin et al. (2013) analyzed the observational results on the mass of the Coma cluster at different distances from the centre using different mass profiles and considering the influence of DE. They concluded that at 1.4 Mpc, the mass is $4.4 \times 10^{14} M_\odot$ (Coma₁), at 4.8 Mpc, $2.6 \times 10^{15} M_\odot$ (Coma₂), and at 14 Mpc, $5.4 \times 10^{15} M_\odot$ (Coma₃). The mass value at 14 Mpc takes into account DE.

The Perseus-Pisces Supercluster. Hanski et al. (2001) derived for the inner part of the PP supercluster the virial mass value of about $1.5 \times 10^{15} M_\odot$ within 2.6 Mpc (PP₁). For the larger region within 22 Mpc (PP₂) the value $8 \times 10^{15} M_\odot$ was obtained from an analysis based on the Tolman-Bondi model including the Λ term.

The Corona Borealis supercluster. Pearson et al. (2014) found that the central parts of the Corona Borealis supercluster (CB) could have a wide mass range of about $0.6 - 12 \times 10^{16} h^{-1} M_\odot$ within a radius of $12.5 h^{-1}$ Mpc, the likely value being around $1 \times 10^{16} h^{-1} M_\odot$. We use the representative values $1.5 \times 10^{16} M_\odot$ within 19 Mpc.

The Laniakea Supercluster. This supercluster (Tully et al. 2014) is the largest well-studied aggregation of matter in the observable universe. According to Tully et al. (2014), the supercluster, if approximated as round, has a radius of 80 Mpc and a mass of about $10^{17} M_\odot$ which comes from the volume and the mean cosmic density. No independent total mass estimate is available.

Also, the region of *dwarf galaxy associations* (DGAs) is shown in the $\log \langle \rho_M \rangle / \rho_\Lambda$ vs. $\log R$ diagram of Fig.2. They have radii ~ 0.3 Mpc and virial masses within $(0.05 - 1) \times 10^{12} M_\odot$ (refs. in Chernin & Teerikorpi 2014). We

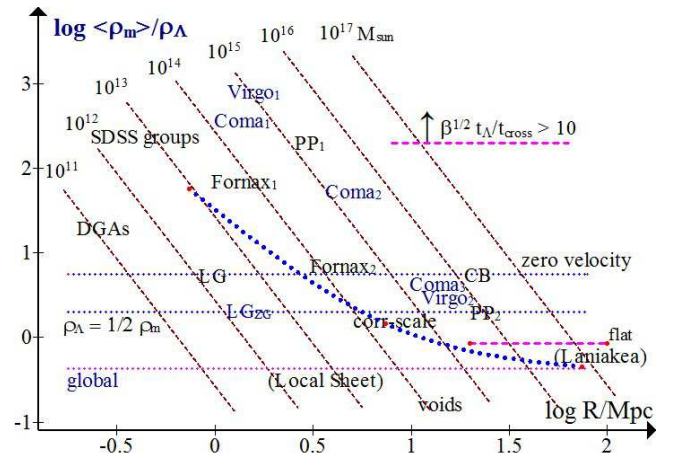


Fig. 2. $\log \langle \rho_M \rangle / \rho_\Lambda$ vs. $\log R / \text{Mpc}$ for example galaxy systems. The inclined lines are for the mass values indicated in M_\odot . The CB supercluster has been slightly shifted to the right. The dotted curve indicates the characteristic mass within radius R as given by the standard 2-point correlation function. The "flat" balance line refers to the limiting case of a flattened system.

have also marked the location ("SDSS groups") around which the galaxy groups (with less than 50 members) extracted from the SDSS-DR10 survey are concentrated (masses from the virial theorem; Tempel et al. 2014).

5. Discussion

The individual objects in Figure 2 represent a heterogeneous collection of examples from the nearby universe. Nevertheless it is interesting to note that the systems are generally found above the "gravity = antigravity" $\langle \rho_M \rangle = 2\rho_\Lambda$ line, which defines the absolute upper size for a gravitationally bound spherical system.

Prominent groups and clusters are usually located deep within the gravity dominated radius (R much less than R_{ZG}), which is also a requirement for them to be virialized. The virial theorem in general form (Chernin et al. 2009) is

$$M = \beta \sigma_V^2 R / G + \frac{8\pi}{3} \rho_\Lambda R^3 \quad (7)$$

where β is a constant \sim unity. Dividing by $(4\pi/3)R^3\rho_\Lambda$ and inserting the timescale $t_\Lambda = (((8\pi/3)G\rho_\Lambda)^{-1/2}$ one obtains

$$\frac{\langle \rho_M \rangle}{\rho_\Lambda} = 2(1 + \beta(\frac{t_\Lambda}{t_{cross}})^2) \quad (8)$$

where the crossing time $t_{cross} = R/\sigma_V$ should be considerably smaller than $t_\Lambda \approx 17 \times 10^9$ yrs for a virialized system. We indicate in Fig.2 the region where $\beta^{1/2} \frac{t_\Lambda}{t_{cross}} > 10$. There also R is $\gtrsim 5$ times smaller than R_{ZG} .

We note that going upwards along a constant- M line makes the influence of the DE on the virial mass determination decrease. It can be shown that the mass derived from Eq.(7) is a factor of $(1 + \alpha(R/R_{ZG})^3)$ larger than the classical result (here $\alpha \sim 1$). The increase is insignificant for well-virialized systems.

In Fig.2 the systems above the "zero-velocity line" (Sect.3) are totally within the collapsing region. The outer

parts of systems below the line have not been retarded down to zero velocity (e.g., the extended Fornax₂, Coma₃, and Virgo₂ systems).

For example, we can read from the diagram that if the mass of the Virgo cluster only would control the dynamics of the Local supercluster up to the distance of the LG, then the zero-gravity distance (at around 11 Mpc) would lie closer than the LG and we would be in the DE dominated region. However, the mass between us and Virgo seems to keep us near the gravity dominated region (Virgo₂ in Fig.2).

The main body of the Corona Borealis supercluster lies in Fig.2 near the zero-velocity line. According to Pearson et al. (2014), this is an example when a supercluster made of several rich clusters may be bound, containing much intercluster matter.

The Local Sheet and the Laniakea supercluster are found below the $\langle \rho_M \rangle = 2\rho_\Lambda$ line. However, the Local Sheet is a strongly flattened system (hence in brackets) and the condition $\langle \rho_M \rangle = 2\rho_\Lambda$ for "gravity = antigravity" at the outer border is not valid.

A flattened system, if viewed as a disc, cannot be bound as a whole if the antigravity force between its centre and the edge (one radius away) is larger than the gravity pulling the edge inward. It is known that a disc exerts a larger gravity force on a particle at its edge than a sphere of the same mass and radius. If the ratio of these forces is $\alpha(>1)$, then Eq.1 leads to the balance condition $\langle \rho_M \rangle = (2/\alpha)\rho_\Lambda$. Therefore the "gravity = antigravity" line should be lowered for a flattened system. Here $\langle \rho_M \rangle$ is the mean density caused by the mass M within the sphere having the radius R (not the mean density of the disc).

For a flat disc, with the density increasing inwards, the ratio $\alpha < 3\pi/4$, while the limiting case of constant density gives $\alpha = 3\pi/4 = 2.35$ (see e.g., Woltjer 1967). In this limiting case, the x coordinate of the balance line in Fig. 2 would be shifted down by 0.37 so that $\langle \rho_M \rangle / \rho_\Lambda = -0.07$ in order to roughly take into account flattened systems.

Chernin et al. (2015) conclude that the Local Sheet is expanding with acceleration and has under-density. This would agree with its location even below the global density line in Fig.2. In fact, the zero-gravity spheres around the LG and nearby groups do not appear to intersect, also suggesting accelerating Hubble recession (Byrd et al. 2012).

The location of the Laniakea supercluster near the "global" line simply reflects the way its mass was estimated from the mean cosmic density by Tully et al. (2014). Even without an independent mass estimate it is clear that the supercluster as a prominent mass concentration hardly can lie below the global line (in the region of voids). On the other hand, if it were to be found near or above the $\langle \rho_M \rangle = 2\rho_\Lambda$ line, its mass had to be the very large $\gtrsim 4 \times 10^{17} M_\odot$, while the large-scale structure formation theory suggests an upper limit of about $10^{16} M_\odot$ for the massive *bound* objects (e.g., Holz & Perlmutter 2012).

The Λ significance diagram may also throw light on the general galaxy field as described by the two-point correlation function (without biasing). With the values generally regarded as standard, i.e. the correlation length $r_0 \approx 5h_{100}^{-1}$ Mpc and the correlation exponent $\gamma \approx 1.75$, we have calculated, as explained in Teerikorpi et al. (2005), typical mass values within the radius R . These have been plotted, as a dashed curve, on the diagram of Fig.2. As already noted by Teerikorpi et al. (2005), the correlation length r_0 is not far from the zero-gravity radius corresponding to the fluctuation described by the correlation function. Beyond r_0 the decreasing fluctuations lie in the DE dominated region, where also the pairwise velocity dispersion of the Hubble flow starts to diminish.

6. Concluding remarks

The $\log \langle \rho_M \rangle / \rho_\Lambda$ vs. $\log R$ diagram is a useful way to characterize systems of galaxies. Different regions in the diagram correspond to the mass and size of a system and its dynamical state within the Λ dominated expanding universe.

The Λ significance graph will be used in forthcoming separate studies to discuss clusters and superclusters, especially as extracted from the SDSS survey. A preliminary inspection of the distribution of SDSS DR7 superclusters shows a range of $\langle \rho_M \rangle / \rho_\Lambda$ and an interesting dependence on the size and morphology of the system, which also can be studied using simulated systems.

Acknowledgements

We thank G. Bisnovatyi-Kogan, L. Liivamägi and E. Saar for useful discussions. ME was supported by the ETAG project IUT26-2 and by the European Structural Funds grant for the Centre of Excellence "Dark Matter in (Astro)particle Physics and Cosmology" TK120.

References

- Byrd, G.G., Chernin, A.D., Teerikorpi, P., & Valtonen, M.J. 2012, *Paths to Dark Energy: Theory and Observation* N.Y., de Gruyter
- Byrd, G.G., Chernin, A.D., Teerikorpi, P., & Valtonen, M.J. 2015, Observations of General Relativity at strong and weak limits. in: General Relativity: The most beautiful of theories. Applications and trends after 100 years, ed. C. Rovelli, De Gruyter Publ.House (Berlin 2015); arxiv.org/pdf/1411.5860
- Chernin, A.D. 2001, Physics-Uspekhi 44, 1099
- Chernin, A.D., & Teerikorpi, P. 2014, Astron. Reports 58, 1
- Chernin, A.D., Nagirner, D.I., & Starikova S.V. 2003, A&A 399, 19
- Chernin, A.D., Emelyanov, N.V., & Karachentsev, I.D. 2015, MNRAS (in press)
- Chernin, A.D., Teerikorpi, P., Valtonen, M.J., et al. 2009, A&A 507, 1271
- Chernin, A.D., Teerikorpi, P., Valtonen, M.J., et al. 2012, A&A 539, A4
- Chernin, A.D., Bisnovatyi-Kogan, G.S., Teerikorpi, P., Valtonen, & M.J.Byrd G.G. 2013, A&A 553, A101
- Drinkwater, M. J., Gregg, M. D., & Colless, M. 2001, ApJ 548, L139
- Einstein, A., & Straus E.G. 1945, Rev.Mod.Phys., 17, 120
- Ekholm, T., Lanoix, P., Teerikorpi, P., Fouqué, P., & Paturel, G. 2000, A&A 355, 835
- Hanski, M., Theureau, G., Ekholm, T., & Teerikorpi, P. 2001, A&A 378, 345
- Holz, D.E., & Perlmutter S. 2012, ApJL, L36
- Lynden-Bell, D. 1981, Observatory 101, 111
- McCall, M.L. 2014, MNRAS 440, 405
- Nasonova, O.G., de Freitas Pacheco, J.A., & Karachentsev I.D. 2011, A&A, 532, 104
- Partridge, C., Lahav, O., & Hoffman, Y. 2013, MNRAS 436, 45
- Peirani, S., & de Freitas Pacheco, J.A. 2008, A&A 488, 845
- Pearson, D.W., Batiste, M., & Batuski, D.J. 2014, MNRAS 441, 1601
- Peirani S. & de Freitas Pacheco J.A. 2006, NewAstron. 11, 325
- Planck Collaboration: Ade, P.A.R., Aghanim, M., Armitage-Caplan, C., et al. 2013, A&A 571, A16
- Saarinen, J. & Teerikorpi, P. 2014, A&A 568, A33
- Teerikorpi, P., Bottinelli, L., Gouguenheim, L., & Paturel G. 1992, A&A 260, 17
- Teerikorpi, P., Chernin, A.D., & Baryshev Yu.V. 2005, A&A, 440, 791
- Teerikorpi, P., & Chernin A.D. 2010, A&A 516, 93
- Tempel, E., Tamm, A., Gramann, M., et al. 2014, A&A 566, A1

Tully, R. B., Courtois, H., Hoffman, Y., & Pomarède, D. 2014, *Nature*,
513, 71

Tully, R.B. 2015, *AJ* 149, A54

van den Bergh, S. 1999, *A&ARv* 9, 273

Woltjer, L. 1967, in *Lectures in Applied Mathematics*, Vol. 9, p.1
(American Mathematical Society, 1967)